IEEE Access
Multidisciplinary | Rapid Review | Open Access Journal

Received July 7, 2020, accepted July 22, 2020, date of publication July 28, 2020, date of current version August 11, 2020.

*Digital Object Identifier 10.1109/ACCESS.2020.3012438*

# Application of Three-Dimensional Laser Scanning in the Protection of Multi-Dynasty Ceramic Fragments

**ENSHENG LIU[1,2], XIAOJUN CHENG[1,3], XIAOLONG CHENG[4], TENGFEI ZHOU[1,3], AND YUHUA HUANG[2]**

[1]College of Surveying and Geo-Informatics, Tongji University, Shanghai 200092, China
[2]College of Building Engineering, Jing Gang Shan University, Ji'an 343009, China
[3]Key Laboratory of Modern Industry Surveying, National Administration of Surveying, Mapping and Geoinformation, Shanghai 200092, China
[4]School of Architectural and Surveying and Mapping Engineering, Jiangxi University of Science and Technology, Ganzhou 341000, China

Corresponding author: Ensheng Liu (les99_ok@126.com)

This work was supported by the National Natural Science Foundation of China under Grant 41671449.

**ABSTRACT** The number of fragments and the variety of primitive cultural relics unearthed in archaeology, especially the mixed fragments of several dynasties unearthed in Qinglong town, Shanghai, pose a great challenge to the manual splicing. The traditional manual comparison method is easy to cause the second damage to the cultural relics. In this paper, the edge feature is extracted based on removing the noise of point cloud, a bilateral filtering point cloud denoising algorithm based on salient features is proposed. By changing the step size and field of view, the Improved Artificial Fish Swarm Algorithm is used to get the matching strategy, and the point cloud is used to reconstruct 3D model by the Dual Quaternion Transformation method. The pairing of fragments and virtual reconstruction can effectively avoid the secondary damage of cultural relic fragments. It provides a feasible artificial intelligence solution for the protection and restoration of similar archaeological excavations.

**INDEX TERMS** Feature extraction, improved artificial fish swarm algorithm, 3D laser scanning, global pairings.

## I. INTRODUCTION

Taking the site of Qing long town in Shanghai as an example, more than 6000 pieces of restorable porcelain and hundreds of thousands of fragments from kilns in Province Fujian, Zhejiang and Jiangxi have been discovered during the six-year archaeological exploration. Most of the porcelain was produced in the southern kilns. The Yue, Deqing and Changsha kilns dominated the Tang Dynasty, and by the Song Dynasty it had been transformed into the Yiyao, Longquan Celadon and Jingdezhen Kilns in Fujian province. The unearthed Tang Dynasty debris heaps are bowls, pots, and so on. The research on the matching of cultural relic fragments and virtual reconstruction is helpful to reduce the secondary damage caused by manual splicing. Fragments belonging to different artifacts were mixed together, and the manual sorting and pairings work is huge, and the challenges are shown in Figure 1.

The associate editor coordinating the review of this manuscript and approving it for publication was Zhihan Lv.

**FIGURE 1.** A large number of fragments unearthed in Qing long town, Shanghai.

In order to minimize the secondary damage caused by manual hand-holding of the fragments, the point cloud data of the fragments are obtained by non-contact 3D laser scanning.

Then, the improved artificial fish school algorithm is used to obtain the matching information of the fragments to assist the conservation and restoration of the cultural relics.

With the development of 3D laser scanning technology, its application in cultural relics conservation has been frequently preferred [1], [2]. The global pairings of fragments arrange each fragment according to the pairings of fragment contour feature, internal geometry feature and color texture. However, the traditional image mosaic method often uses the sub-image fusion method, the efficiency of this method can be evaluated by the similarity of specific features. Zhang *et al.* [3] proposed a greedy algorithm for 2D fragment assembly by repeatedly assembling two neighboring fragments into a composite one. It provided an idea for the mosaic of cultural relic fragments, but the application of this algorithm to the mosaic of three-dimensional fragments is still unclear. Real models often include rich texture information, which can compensate for the limited shape information [4]. Pintus [5] presented a review of recent techniques for performing geometric analysis in cultural heritage applications. Their method utilizes the texture and color characteristics of the vessel fragments as well as other factors including expert historical knowledge of the period, site location, and provenance of the artifact. Cohen *et al.* [6] presented a theory for automatically reconstructing fragments. Their system completes the reconstruction by first segmenting the fragments into a set of faces bounded by sharp curves, then computing multi-scale surface characteristics, and pairings based on techniques of forwarding search and surface consistency. Son *et al.* [7] proposed a novel approach to automatically match the fragments. They scan the mixed and unorganized fragments from three pots and then estimate the axis of symmetry for each fragment through analyzing the point cloud. Besides, break curves of the fragments are also extracted. The symmetry property and break curve information derived are then applied to match.

The previous approaches all can be implemented under a certain condition. When some fragments are missing, which is common for cultural relics, errors may occur during pairings. Many previous works extracted boundaries for pairings. However, the procedure of boundary curve smoothing is often time-consuming. Moreover, the pairings of fragments is a procedure of reconstructing the initial model of the object which needs to take the global consistency of different results into consideration.

From the perspective of combinatorial mathematics, fragments pairings problem is equivalent to combing and all the fragments according to certain rules, namely, finding the correspondence relations among all fragments [8]. Therefore the problem can be considered as a combinatorial optimization problem, and one of the approaches to solving the combinatorial optimization problem is enumeration method. However, the combination explosion problem may occur when there are large amounts of fragments. So, the global pairings of 3D fragments problem is a combinatorial optimization problem with characteristics of large scale, nonlinear and multi-objective.

## II. MATERIAL AND METHODS

To testify the efficiency of the proposed method, an experiment has been carried out. The experimental objects are some fragments of earthenware and two porcelains from different dynasties.

Each fragment is assumed to be an element of a collection, and the characteristics of the fragment itself can be considered as several constraints. The following three reasons account for the vagueness and incompleteness of constraints. (1) Deformation and inaccurate edge information often appear in each fragment due to extrusion from external force and wear and erosion. Sometimes, certain fragments are also missing. (2) The point cloud data are incomplete due to the performance of the scanner, the occlusion, and the unavoidable defects of the scanning method. (3) Errors may occur during the process of extracting features. To match the fragments is to find the best solution under constraints. However, the incompleteness of the constraints often leads to inaccurate corresponding relations. So it is necessary to analyze the constraints, namely, finding knowledge from uncertain information by the reduction model extension as the basis of fragments pairings [9].

In the research, the information acquired is often imprecise, incomplete and vague, which includes a lot of uncertainty. It is rather difficult to find the corresponding relations among fragments due to the vagueness and incompleteness of the constraints. Some artificial intelligence (AI) algorithms are very similar to the research of element classification combination and fragment matching. Particle Swarm Optimization (PSO) is a widely studied algorithm. However, the PSO is not good at maintaining population diversity, which usually leads to premature convergence or local optimization [10]. The superior solution set search problem contains parameters that provide constraints on evaluation value and distance. Fukushima *et al.* [11] proposed an evaluation indicator that is inspired by a method based on a dominance relation in multi-objective optimization problems. Bouamama *et al.* [12] presented an efficient random iterative greedy algorithm for solving a class of problems related to the random local search strategy of the greedy algorithm. Although the multilevel framework cannot be considered as a panacea for combinatorial problems, it can provide an extremely useful addition to the combinatorial optimisation toolkit [13]. Ant Colony Algorithm (ACO) is also used to solve the optimal solution. Despite its successes, ACO is not a perfect algorithm: it can remain trapped in local optima, miss a portion of the solution space, or in some cases, it can be slow to converge [14], [15].

In this paper, a global pairings approach based on an Artificial Fish School Algorithm (AFSA) is adopted to solve the problem. The process can be seen as the school of fish foraging for food. In a water area, fishes are most likely distributed around the region where foods are most abundant and nutritional [16]. ASFA has the advantages of fault tolerance of parameter setting, insensitivity to initial value and parallelism. So it is suitable to solve nonlinear programming and multiple objective programming problems [17], [18].

First, reflect the feature pairings scheme space into a coding space using the binary encoding mechanism. Under the given constraints, ASFA is used to search the coding space and get the optimal resolution. All possible pairings could be reflected by coding mechanism (based on fracture surface), thus, these codes can be seen as a shoal of fish. Some other AI methods, e.g., ACO and bacterial foraging algorithm have also been the research focus recently [19]. Not only can the ASFA modify the current pairings scheme during the process, but also can it obtain the optimal solution.

## III. POINT CLOUD PROCESSING AND FEATURE EXTRACTION FOR 3D SCANNING OF DEBRIS

### A. REMOVAL OF NON-RELIC DEBRIS POINTS FROM LASER 3D SCANNING

There are many mature algorithms to extract the edge, color and geometry information of debris point cloud [20], [21]. The methods of feature points and boundary extraction in this study are based on references. But processing the scanned point cloud data in advance is a very important process. In fact, the noise is often distributed irregularly around the debris, making it difficult to distinguish using a single mathematical model.

The noise of scattered point cloud can be divided into three types: (1)The point cloud which deviates from the debris point cloud and is suspended above the debris point cloud has little correlation with the measured object, which can be regarded as the error points; (2) The point cloud which is far from the center of debris and is dense in different sizes; (3)The noise point is mixed with the correct point of the fragment.

For the first and second kinds of points, the point cloud was divided into three parts according to x, y and z. Then the grid position of each point is obtained, and the number of point clouds in each grid is determined. The minimum coordinates of a space cube bounding box are $x_{min}$,$y_{min}$, $z_{min}$, the maximum coordinates are $x_{max}$,$y_{max}$,$z_{max}$, the length of the side of the cube is l, then the number of cubic grids in the x, y, and z directions is:

$$N_1 = int\left\{\frac{1}{l}\left[(x_{max}+e)-(x_{min}-e)\right]\right\}+1 \quad (4.1)$$

$$N_2 = int\left\{\frac{1}{l}\left[(y_{max}+e)-(y_{min}-e)\right]\right\}+1 \quad (4.2)$$

$$N_3 = int\left\{\frac{1}{l}\left[(z_{max}+e)-(z_{min}-e)\right]\right\}+1 \quad (4.3)$$

Let the three-dimensional coordinates of a given point be $p_x$, $p_y$, and $p_z$, then the grid of the cube in which it is located is a hash function:

$$I = int\left[\frac{1}{l}(p_x - x_{min})\right] \quad (4.4)$$

$$J = int\left[\frac{1}{l}(p_y - y_{min})\right] \quad (4.5)$$

$$K = int\left[\frac{1}{l}(p_z - z_{min})\right] \quad (4.6)$$

In the above equations (4.4, 4.5, 4.6), I, J and K are the index numbers of the cube grid in the x, y and z axes of the cube where the point is located. One-dimensional array of storage pointers is used to record the ordinal number of all data points in each grid.

The K-Nearest Neighbor (KNN) of the current grid search point p are arranged in ascending order of distance. If the K neighbors of the candidate points in the current grid have been found, and the distances are all less than the shortest distance between the point p and the six faces of the grid, then the search for the KNN of the candidate points is over, when $K$ value is $15 \sim 25$, the effect is better [22]. After the scattered point cloud has processed, the number of data points in each small stereo grid is first determined. If the number is less than 2, all data points in the grid are deleted. The goal is to find and remove the scattered, sparse data points that hover over the point cloud.

Jones *et al.* [23] improved the algorithm of bilateral filter in image processing and applied it to the processing of 3D model. The anisotropic smoothing denoising algorithm based on the bilateral filter is simple and fast, but it is easy to have the problem that the feature is over-smoothed. In addition, some scholars have improved the method and obtained a better de-noising effect on the model of the turbofan [24], [25]. The edge of the bilateral filter to retain better, and Vinax filter and Gaussian filter noise removal will be clear of the edge, for high-frequency details of the protection is not obvious. But there are also some shortcomings, for example, for the regional gradient transformation of point cloud data, the effect is unsatisfactory. For the third kind of point cloud noise, a bilateral filtering point cloud denoising algorithm based on salient features is proposed. The bilateral filtering method is defined as $p_i^{\cdot} = p_i - \varepsilon n$, where $p_i$ is point clouds obtained directly from 3D laser scanning, $p_i^{\cdot}$ is de-noised points. n is the normal direction, $\varepsilon$ is a bilateral filter factor. Let $p_j = KNN(p_i)$ is the neighborhood point of $p_i$.

$$\varepsilon = \frac{\sum_{p_j}\omega_1\left(\left\|p_j - p_i\right\|\right)\omega_2\left(\left|\langle n_j - n_i\rangle - 1\right|\right)(n, p_j - p_i)}{\sum_{p_j}\omega_1\left(\left\|p_j - p_i\right\|\right)\omega_2\left(\left|\langle n_j - n_i\rangle - 1\right|\right)} \quad (4.7)$$

$\omega_1$, $\omega_2$ are the weights of the spatial domain (the Gauss filter on the micro-tangent plane in the local neighborhood of the sampling point) and the weights of the eigenvalues (the Gauss filter with normal vector change in the local neighborhood of the sampling point), respectively. The former is used to control smoothness, and the latter can determine the degree of feature retention.

$$\omega_1(x) = e^{-\frac{x^2}{2\delta_1^2}} \quad (4.8)$$

$$\omega_2(y) = e^{-\frac{y^2}{2\delta_2^2}} \quad (4.9)$$

$\delta_1$ is the influence factor of the distance from the sample point to its neighborhood, and the value of $\delta_1$ has an effect on the filtering result. The larger the value the more


(a)Debris cloud from 3D laser scan (b)Removing the noise point cloud (c)Debris cloud deviation

**FIGURE 2.** Sample debris cloud de-noise processing.

neighborhood midpoints of the sample point are, and the denoising result is better, but the effect of feature maintenance in point cloud model is reduced. $\delta_2$ is the influence factor of the normal upward projection of the distance vector which from the sampling point to the point in the neighborhood, the bigger the feature, the better the retention. The specific formulas for the two parameters are as follows:

$$\delta_1 = \max \left\| p_j - p_i \right\| ; i \in [1,n] \tag{4.10}$$

$$\delta_2 = \sqrt{\frac{1}{n-1} \sum_{i=1}^{n} (\mu_i - \bar{\mu})^2} \quad (\mu = \langle p_j - p_i, n \rangle) \tag{4.11}$$

Using the above methods, we remove the noise point cloud as shown in Figure 2.

### B. EDGE EXTRACTION OF DEBRIS POINT CLOUD

Get one point p and its KNN $N_j$ ($j = 1, 2, 3, \ldots, k$) as a local reference. Then using the Least Squares to fit the micro-tangent plane. The plane is represented by the following formula.

$$\begin{bmatrix} x_1 & y_1 & z_1 & 1 \\ x_2 & y_2 & z_2 & 1 \\ \ldots & \ldots & \ldots & \ldots \\ x_k & y_k & z_k & 1 \end{bmatrix} \begin{bmatrix} a_1 \\ a_2 \\ a_3 \\ a_4 \end{bmatrix} = 0 \tag{4.12}$$

Assume $\begin{bmatrix} x_1 & y_1 & z_1 & 1 \\ x_2 & y_2 & z_2 & 1 \\ \ldots & \ldots & \ldots & \ldots \\ x_k & y_k & z_k & 1 \end{bmatrix} = A$, $a = [a_1, a_2, a_3, a_4]^T$, therefore $Aa = 0$. Singular value decomposition on $A^TA$:

$$A = U \begin{bmatrix} \Delta & 0 \\ 0 & 0 \end{bmatrix} V^H \tag{4.13}$$

U and V are unitary matrices in the formula, $\Delta = \text{diag}\left[\sqrt{t_1}, \sqrt{t_2}, \ldots, \sqrt{t_r}\right]$ ($i = 1,2,\ldots, r$), where $t_i$ is the positive eigenvalue of $A^TA$, r is the number of singular values. The eigenvector corresponding to the minimum eigenvalue of $A^TA$ is the least square solution of $Aa = 0$, and the normal vector of the micro-tangent plane is $n = (a_1, a_2, a_3)$. Projection point coordinates can be calculated by the projection point $p'$ and $N_j'$ from the micro-tangent plane. Suppose the scattered point set coordinates are $(x_i, y_i, z_i)(i = 1,2,\ldots, n)$, the projection point on the micro-tangent plane has the coordinates $\left(x_i', y_i', z_i'\right)$.

$$a_1 x_i' + a_2 y_i' + a_3 z_i' + a_4 = 0 \tag{4.14}$$

$$\frac{\left(x_i' - x_i\right)}{a_1} = \frac{\left(y_i' - y_i\right)}{a_2} = \frac{\left(z_i' - z_i\right)}{a_3} = m \tag{4.15}$$

where,

$$m = \frac{a_1 x_i + a_2 y_i + a_3 z_i}{\sqrt{a_1^2 + a_2^2 + a_3^2}}$$

The coordinates of the projection point can be obtained from Equations (4.14) and(4.15). On the micro-tangent plane, the vector direction from $p'$ to the point farthest from $p'$ is x-axis, and the direction perpendicular to x-axis is y-axis. For the sample points projected on the micro-tangent plane, if the K-neighborhood projection points are uniformly distributed around the sample points, then the sample points are non-boundary points, otherwise the sample points are boundary feature points. The edge of the fragment can be fitted by these feature points, and a series of corners can be marked as shown in Figure 3.

## IV. COMPARISON OF ARTIFICIAL INTELLIGENCE ALGORITHMS AND FRAGMENT GLOBAL PAIRINGS BASED ON IMPROVED ASFA

Since each edge of the grid is shared by at most two facets, the grid is manifold, therefore, we use a half-edge data structure. Assume that when a complete cultural relic breaks, it has n pieces of fragments. These fragments can be expressed by a set $G_A$, and $G_A = \{T_{A1}, T_{A2}, \ldots, T_{Ai}, \ldots, T_{An}\}$, $i = 1$ to $n$, $T_{Ai}$ is the fragment numbered $i$ and has several fractured surfaces. The major test objects of this research are thin-walled cultural relics, so the fractured surface can approximately be seen as a verge that can best reflect its feature. The fractured surfaces of $T_{Ai}$ can be expressed by a set $L_{Ai}$, and $L_{Ai} = \{l_{Ai1}, l_{Ai2}, \ldots, l_{Aii}, \ldots, l_{Ain}\}$.

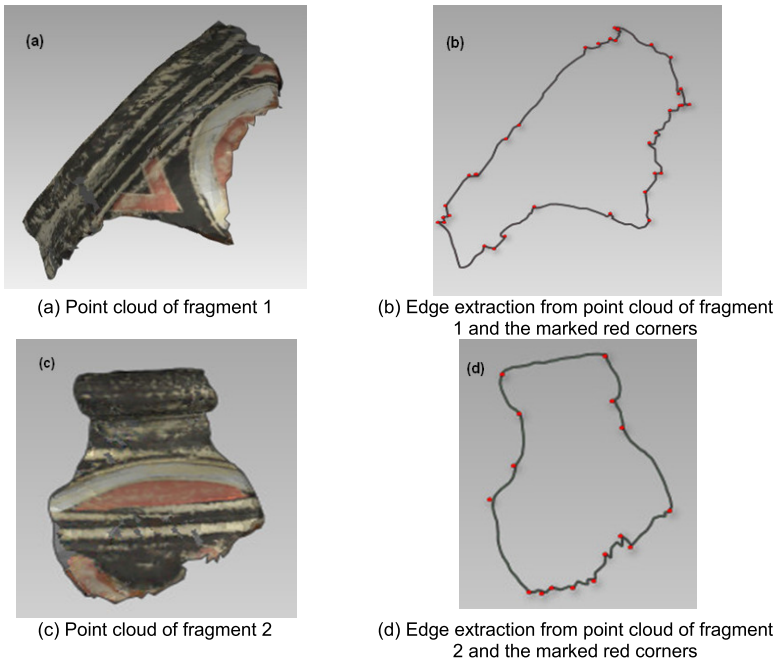


(a) Point cloud of fragment 1

(b) Edge extraction from point cloud of fragment 1 and the marked red corners

(c) Point cloud of fragment 2

(d) Edge extraction from point cloud of fragment 2 and the marked red corners

**FIGURE 3.** **Sample fragment edge extraction and the marked corners.**

During the process of pairings, any two of the fractured surfaces can be matched. However, the fractured surfaces belonging to a single fragment cannot be matched. The whole possible pairings of the fractured surfaces can be expressed by a matrix $M = (T_{Aij})_{n\times n}$,where $n$ is the total number of the fractured surfaces, $i$, $j$ are the sequence number of the fractured surfaces.

$T_{Aij}$ is a symmetric matrix. To reduce the storage space, only the half triangular matrix needs to be stored. In this experiment, the lower triangular matrix is used.We want to get the possible matching conditions in the matching scheme. However, this algorithm can only have one optimal pairing scheme. So this is the key step in determining the value of $T_{Aij}$. The current state of a single fragment can be expressed by a vector $V = (x_1, x_2, \ldots, x_n)$, where $x_i$ is a variable of optimizing and the objective function $F(x)$. The results were influenced by edge features, geometric features, texture features and the knowledge of the archaeologist [6]. Here the impact factors are regarded as visual factors and when they acquire the visual condition, they will approach the value of the objective function by a shift step.

In the process, each fragment has multiple features, and it's easy to approach the fragments with similar features. Although the behaviors seem to be jumbled, the approaching behavior is in order and purposeful [26]. Let $V_i^{'}$ be the state after optimizing, and $V_i$ be the current state, then the process of optimizing can be expressed as follows:

$$V_i^{'} = V_i + \text{visual} \cdot \text{rand}(), i = n \cdot \text{rand}() \tag{5.1}$$

$$V_{\text{next}} = \frac{v_i^{'} - v_i}{\left\| v_i^{'} - v_i \right\|} \cdot \text{step} \cdot \text{rand}() \tag{5.2}$$

The search range of the AFSA is determined by the field of view parameters. Under the fixed condition, only a few individuals are different from the optimal solution when the individuals approach the optimal solution gradually, if the algorithm is still searching in the original field of view, it will be inefficient, so in this case, we should narrow down the search area. When the field of view is smaller, the local search ability of the algorithm is strong, so the convergence speed of the algorithm is slow and the computation is large. When the convergence speed of the algorithm is accelerated, the global search ability is enhanced, and it is easy to skip the optimal solution. In order to improve the global search ability and convergence speed of the algorithm, a larger field of view is adopted in the early stage of the algorithm. Too small search range also affects the optimal solution, so the search range is adjusted dynamically by formula (5.2) in the iteration.

$$\begin{cases} \text{visual}_i = \text{visual}_{i-1} \times \exp(-\left(\dfrac{i}{n}\right)^2) \\ \text{visual}_i = \text{visual}_{\min}, \text{visual}_i \le \text{visual}_{\min} \end{cases} \tag{5.3}$$

where i is the current iteration number, n is the maximum iteration number which needs to be set according to the effect of the Algorithm, and visual is the current field of view. The step size determines the convergence speed of the algorithm, and the larger the step size, the faster the earlier convergence speed, but sometimes there will be oscillation phenomenon. Therefore, the step length is dynamically adjusted according to formulas (5.3).

$$\begin{cases} \text{step}_i = \text{step}_{i-1} \times \exp(-\left(\dfrac{i}{n}\right)^2) \\ \text{step}_i = \text{step}_0, \text{step}_i \le \text{step}_0 \end{cases} \tag{5.4}$$

The initial value is namely step, which converges quickly in the early stage by changing step size, and can be searched more carefully in the later stage, thus improving the efficiency of finding the optimal solution. The congestion factor will affect the local extremum of the algorithm, and an exponential decay strategy is used to calculate the crowding factor during the iteration ($\alpha$ is the attenuation factor, and $\delta$ is the congestion factor):

$$\delta_{i+1} = \alpha \times \delta_i \quad (0 < \alpha < 1) \tag{5.5}$$

Thus, the algorithm gains a better ability to avoid falling into a optimal solution.

$$X_i^{\cdot} = X_i + \text{step}_i^{\cdot} \times \delta_{i+1} \tag{5.6}$$

The thresholds of these four visual factors can be set separately. Select a fragment randomly and compare its certain feature with all the other fragments. If two fragments can match then return 1, conversely, then return 0. In the computation process, the matched pairs can be optimized and adjusted. Therefore, this algorithm can obtain global information and perform global pairings as shown in Figure 4.

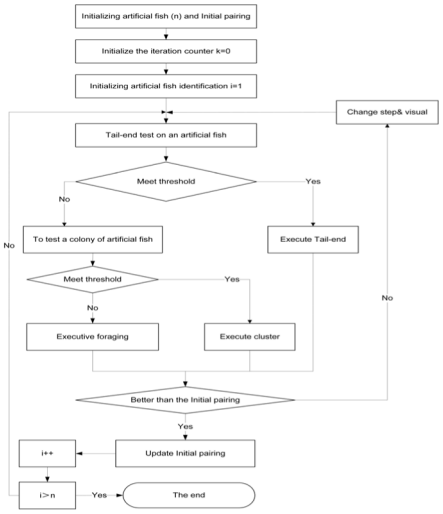


**FIGURE 4.** The flow chart IAFSA.

The threshold minimum value is named as $X_{min}$ and the maximum value is $X_{max}$. The $X_{random}$ is selected randomly between $X_{min}$ and $X_{max}$. For example, it's easy to distinguish among the pieces of different dynasties is a piece of pottery or porcelain, which can be set to a larger field of view when foraging for food. The size of different objects is related to the size of the original objects, so the geometric features of the objects with significant size difference are clearly distinguished, and the small visual field is helpful to improve the search efficiency and accuracy. The superior individual is reserved and the worst individual is eliminated in every generation, as shown in Table 1.

Nowadays, there are many mature artificial intelligence algorithms, but not all of them are suitable for the problems we solve today. It is necessary to converge as soon as possible

**TABLE 1.** Algorithm.

| | |
|---|---|
| for i = 1:N<br>Pair = [X(i,1),X(i,2)];<br>d(i) = maxf(Pair);<br>while(i≤n)<br>for i = 1:N<br>Pair = [X(i,1),X(i,2)];<br>for j = 1:N<br>Pair _1 = [X(j,1), X(j,2)];<br>if (norm(Pair _1- Pair)<Visual)<br>nf1 = nf1+1;<br>Xc = Xc+ Pair _1;<br>end | If( $\mathbf{X}_1' > \mathbf{X}_2'$ ) $\{\mathbf{X}_{\mathbf{better}}' = \mathbf{x}_1'; \mathbf{X}_{\mathbf{worse}}' = \mathbf{x}_2';\}$<br>Else $\{\mathbf{X}_{\mathbf{better}}' = \mathbf{x}_2'; \mathbf{X}_{\mathbf{worse}}' = \mathbf{x}_1';\}$ End if<br>If (Y($\{\mathbf{Y}_{\mathbf{better}}' = \mathbf{Y}(\mathbf{max})\}$))<br>$\{\mathbf{X}_{\mathbf{max}} = \mathbf{X}_{\mathbf{better}}'\}$ End if<br>If (Y($\mathbf{X}_{\mathbf{worse}}'$)> $\boldsymbol{Y}(\mathbf{X}_{\mathbf{min}})$)<br>$\{\boldsymbol{X}_{\boldsymbol{min}} = \mathbf{X}_{\mathbf{worse}}'; \mathbf{X}_{\mathbf{random}} = \mathbf{X}_{\mathbf{better}}';\}$<br>Else if (Y($\mathbf{X}_{\mathbf{better}}'$)> $\boldsymbol{Y}(\mathbf{X}_{\mathbf{min}})$)<br>$\{\mathbf{X}_{\mathbf{min}} = \mathbf{X}_{\mathbf{better}}';\}$ End if<br>End if<br>Output: Optimal $\mathbf{X}_{\mathbf{min}}$ and $\mathbf{X}_{\mathbf{max}}$ |

in advance, taking into account some uncertainties. We need some simulation experiments to compare the advantages and disadvantages of common algorithms. We randomly extract point cloud data from the fragments and compare the convergence performance of four common algorithms. Here we take a sample of 80 edges from 16 fragments,as shown in Table 2.

## V. EXPERIMENT AND RESULTS

The length of the edge is selected as the visual factor, there are 80 edges corresponding to 16 pieces of debris, and the step size is 0.83 (the ratio of the length of the two sides is not greater than 0.83). Under the constraint of $\delta$, 16 fracture edges of artifact A are compared, and the possible matching matrix is obtained as follows:

$$T_{Aij} = \begin{bmatrix}
0 & & & & & & & & & & & & & & \\
0 & 0 & & & & & & & & & & & & & \\
0 & 0 & 0 & & & & & & & & & & & & \\
0 & 0 & 1 & 0 & & & & & & & & & & & \\
0 & 0 & 1 & 0 & 0 & & & & & & & & & & \\
0 & 0 & 1 & 0 & 0 & 0 & & & & & & & & & \\
0 & 0 & 0 & 1 & 1 & 1 & 0 & & & & & & & & \\
0 & 0 & 0 & 1 & 1 & 1 & 0 & 0 & & & & & & & \\
0 & 0 & 0 & 0 & 0 & 0 & 0 & 0 & 0 & & & & & & \\
0 & 0 & 1 & 0 & 1 & 1 & 1 & 1 & 0 & 0 & & & & & \\
0 & 0 & 0 & 1 & 0 & 1 & 1 & 1 & 0 & 0 & 0 & & & & \\
0 & 0 & 0 & 1 & 1 & 0 & 1 & 1 & 0 & 1 & 0 & 0 & & & \\
1 & 1 & 0 & 0 & 0 & 0 & 0 & 0 & 0 & 0 & 0 & 0 & 0 & & \\
0 & 0 & 0 & 1 & 0 & 1 & 1 & 0 & 0 & 0 & 1 & 0 & 0 & 0 & \\
0 & 0 & 0 & 1 & 0 & 1 & 1 & 1 & 0 & 1 & 1 & 0 & 0 & 1 & 0 \\
0 & 0 & 0 & 0 & 0 & 0 & 1 & 1 & 0 & 0 & 1 & 0 & 0 & 1 & 0 & 0
\end{bmatrix}$$

All the possible pairings are further confirmed, and the possible ones are retained while the impossible ones are removed by the Eq.(5.4). Transform the value of the visual factor. Select the medium value of the fitting radius of the fragment, step equals to 0.9, and perform further optimization of the above matrix under the restraint. Transform the visual factor again. Select color texture as the pairings requirements, and perform optimization. For instance, if one fractured surface is colored, then, the fragment pairings it is sure to be colored. The color feature can be calculated by gray value.

**TABLE 2. Comparison of cvergence performance of four algorithms.**

| Number of iterations | I ASFA(time: s) | PSO(time: s) | GA(time: s) | ACO(time: s) |
|---|---|---|---|---|
| 0 | 460 | 450 | 450 | 440 |
| 10 | 420 | 400 | 410 | 410 |
| 20 | 340 | 375 | 350 | 370 |
| 30 | 310 | 340 | 335 | 340 |
| 40 | 308 | 330 | 325 | 318 |
| 50 | 302 | 320 | 320 | 308 |
| 60 | 302 | 320 | 315 | 308 |
| 70 | 302 | 320 | 315 | 308 |
| 80 | 302 | 320 | 315 | 308 |
| 90 | 302 | 320 | 315 | 308 |
| 100 | 302 | 320 | 315 | 308 |

The fragments belonging to artifact A is more sensitive to the color texture information. The step value 0.2 shows that the matrix can be optimized only by a small part of non-white color in the edge.

Through the matrix the pairings information can be obtained, and the possible pairings pairs are as follows:

$$T_{Aij} = \left\{ \begin{array}{l} (T_{A13}, T_{A26}), (T_{A13}, T_{A411}), (T_{A24}, T_{A513}), \\ 0, (T_{A24}, T_{A514}), 0, \\ (T_{A25}, T_{A612}), (T_{A25}, T_{A615}), (T_{A26}, T_{A38}), \\ (T_{A26}, T_{A615}), (T_{A38}, T_{A512}), (T_{A37}, T_{A616}), \\ (T_{A411}, T_{A514}), (T_{A411}, T_{A616}), (T_{A514}, T_{A616}) \end{array} \right\}$$

By the optimization of visual factor, the unique matched pair $(T_{A37}, T_{616})$ can be obtained. Then this pair is regarded as a confirmed pair, other pairs as $(T_{A411}, T_{A616})$, $(T_{A514}, T_{A616})$, $(T_{A13}, T_{A411})$, $(T_{A24}, T_{A513})$, $(T_{A26}, T_{A38})$, $(T_{A26}, T_{A615})$, $(T_{A25}, T_{A615})$ are then removed. Fragments $T_{A11}$ and $T_{A12}$ don't have a pairings result but $T_{13}$ is matched. The main results showed as follows:

$$T_{Aij} = \left\{ \begin{array}{l} (T_{A13}, T_{A26}), (T_{A24}, T_{A513}), (T_{A25}, T_{A615}) \\ (T_{A38}, T_{A512}), (T_{A37}, T_{A616}), (T_{A411}, T_{A514}) \end{array} \right\}$$

It is clear that the changes of visual factor and step can gradually optimize the pairings matrix and can obtain enough matched pairs satisfying pairings requirements. During the process all the possible pairings have been analyzed. The results can guide the pairings of fragments in real life in case of secondary damage to the cultural relic. According to results $T_{Aij}$, the 3D models of the original artifacts need to be reconstructed through rigid transformation. The Iterative Closest Point algorithm proposed by Besl and McKay [27] can be performed between two point clouds. There is no common point cloud between the two pieces of debris, and sometimes the edge will be worn, ICP algorithm is not ideal here. Moreover, non-rigid point cloud registration [28], [29], and the 4-Points Congruent Sets Algorithm [30], [31] has some limits like equiaxed distortion and overlapping which is not available for the fragments. So, the Dual Quaternion Transformation (DQT) method is utilized in this paper to reconstruct the point clouds [32]. The DQT (6.1) and (6.2), as shown at the bottom of the page.

Here R is the standard $3 \times 3$ orthogonal rotation matrix. After the initial attitude correction with Seven-parameter Transformation, the precise point cloud splicing was carried out. To test the effect of the DQT rotation on rigid body motion, we applied matlab12b to computer with CPU of Inter R Core TM i5-4200H and Ram of 8G. In this paper, 100 randomly generated 3D coordinate points $p_i = (x_i, y_i, z_i)^T$, $0 \leq (x_i, y_i, z_i) \leq 400$ are used as the piecewise point set models. Firstly the vectors that go around the origin direction are (3.0,4.0,5.0) and rotate 65 degrees in a straight line, then translate (5.0,6.0,7.0)as the target fragment point set $p_i' = \left(x_i', y_i', z_i'\right)^T$. Singular Value Decomposition(SVD) and Quaternion are compared with the DQT in this paper.

The experiment was divided into two steps. In the first step, we verify the computational accuracy of the algorithms under different noise levels. We input 20 different sets of 50 points and run each set 20 times. Gauss noise with different standard deviation (mean 0) is added to the transformed point coordinates each time, which is used as the corresponding target feature point. From the experimental results given in table 3, we can see that the dual quaternion method and the SVD have similar performance at the lower noise level, but with the increasing noise level, the DQT has better performance than the SVD, performs better in motion parameter estimation, and better performance in general. In the second step, we maintain the standard deviation of gauss noise at 0.5, and select a different number of points, execute each set 20 times. The converted angular and translational standard deviation results are given in Table 4.

It can be derived from Table 4 that with the increase of the number of randomly selected points in the point set, it is expected that the Quaternion method and DQT method have no deviation in estimating the rotation parameters. But for the same point, the latter can obviously improve the accuracy of translation parameter estimation. At the same time, Table 3 and Table 4 show that reducing the noise level and increasing the number of feature points can improve the accuracy of motion parameter estimation. According to the

$$q = (q_0, [q_1, q_2, q_3]) \tag{6.1}$$

$$\mathbf{R} = \begin{bmatrix} q_0^2 + q_1^2 - q_2^2 - q_3^2 & 2(q_1q_2 - q_0q_3) & 2(q_1q_3 + q_0q_2) \\ 2(q_1q_2 + q_0q_3) & q_0^2 - q_1^2 + q_2^2 - q_3^2 & 2(q_2q_3 - q_0q_1) \\ 2(q_1q_3 - q_0q_2) & 2(q_2q_3 + q_0q_1) & q_0^2 - q_1^2 - q_2^2 + q_3^2 \end{bmatrix} \tag{6.2}$$

**TABLE 3.** Comparison of standard deviation of motion parameters at different noise levels.

| Standard deviation | Dual Quaternion Transformation | | | | | |
|---|---|---|---|---|---|---|
| | X | Y | Z | $\theta_x$ | $\theta_y$ | $\theta_z$ |
| 0.1 | 0.0432 | 0.0429 | 0.0184 | 0.0025 | 0.0028 | 0.0023 |
| 0.3 | 0.0691 | 0.0687 | 0.0512 | 0.0063 | 0.0057 | 0.0061 |
| 0.5 | 0.1217 | 0.1157 | 0.0973 | 0.0119 | 0.0126 | 0.0124 |
| 0.7 | 0.1713 | 0.1669 | 0.1326 | 0.0163 | 0.0153 | 0.0157 |
| 0.9 | 0.2116 | 0.2089 | 0.1673 | 0.0212 | 0.0225 | 0.0203 |
| Standard deviation | Singular Value Decomposition | | | | | |
| | X | Y | Z | $\theta_x$ | $\theta_y$ | $\theta_z$ |
| 0.1 | 0.0532 | 0.0587 | 0.0253 | 0.0024 | 0.0026 | 0.0023 |
| 0.3 | 0.0974 | 0.1376 | 0.0864 | 0.0068 | 0.0069 | 0.0072 |
| 0.5 | 0.1842 | 0.2652 | 0.1376 | 0.0122 | 0.0123 | 0.0125 |
| 0.7 | 0.2574 | 0.3641 | 0.1943 | 0.0152 | 0.0151 | 0.0152 |
| 0.9 | 0.3213 | 0.4473 | 0.2536 | 0.0217 | 0.0208 | 0.0226 |

**TABLE 4.** Comparison of standard deviation of motion parameters for different points at the same gaussian noise level.

| Number of points | Dual Quaternion Transformation | | | | | |
|---|---|---|---|---|---|---|
| | X | Y | Z | $\theta_x$ | $\theta_y$ | $\theta_z$ |
| 25 | 0.1743 | 0.1635 | 0.1136 | 0.0159 | 0.0161 | 0.0160 |
| 50 | 0.1206 | 0.1149 | 0.0978 | 0.0122 | 0.0124 | 0.0121 |
| 75 | 0.1005 | 0.0984 | 0.0982 | 0.0121 | 0.0119 | 0.0122 |
| Number of points | Quaternion method | | | | | |
| | X | Y | Z | $\theta_x$ | $\theta_y$ | $\theta_z$ |
| 25 | 0.6721 | 0.8763 | 0.5416 | 0.0158 | 0.0162 | 0.0159 |
| 50 | 0.3215 | 0.4327 | 0.2384 | 0.0123 | 0.0125 | 0.0122 |
| 75 | 0.2018 | 0.2257 | 0.1925 | 0.0120 | 0.0121 | 0.0123 |

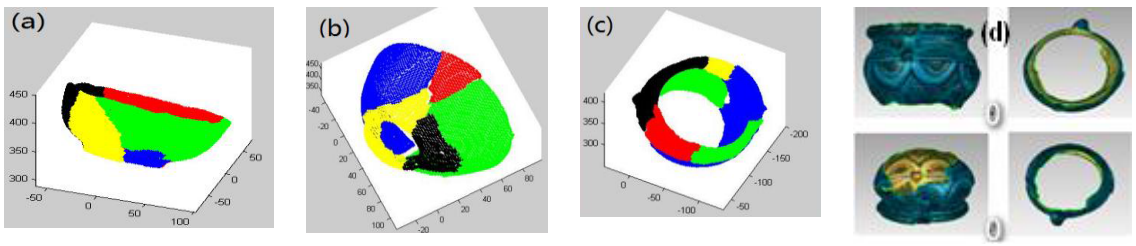


**FIGURE 5.** Results of artifacts point cloud. (a) Artifact A. (b) Artifact B. (c) Artifact C. (d) Four views of a three-dimensional model of C.

results, the transformed point cloud can be obtained through the rigid transforming of the matched fragments point cloud. The fragments belonging to artifact A are transformed to the same coordinate as shown in Figure 5(a). Figure 5(b) and Figure 5(c) show the results of artifact B and artifact C respectively. The texture information is acquired by CCD camera, and the surface information is reconstructed by means of texture correction and texture mapping. We paste the fragment texture to get the reconstructed three-dimensional model of the object, as shown in Figure 5(d) for example.

## VI. CONCLUSION AND FUTURE WORK

A method of global archaeological debris pairings based on AFSA is proposed. The method firstly extracts feature points from the debris cloud points obtained by a 3D laser scanner. By changing the step size and field of view, Improved AFSA is adopted to obtain one-time optimal results by multiple feature search. It can solve the accumulation of errors caused by one-to-many pairings. Besides the application of the algorithm provides a solution for the further development of intelligent debris pairings. we study the pairing question of why these two edges of the two pieces fit together rather than any other. This is rarely mentioned in studies of similar problems. Experimental results show the feasibility and effectiveness of the proposed method. It provides a feasible method for computer-aided reconstruction of the intermingled ceramic fragments of several dynasties.

The algorithm has the following three characteristics: (1) It has fast convergence speed and can be used to solve multi-objective optimization problem; (2) It can be used to get a feasible solution quickly for some situations where the precision is not high, debris with large radius and debris with small radius often do not belong to the same artifact; (3) It does not need the strict mechanism model of the problem or even the exact description of the problem, when certain features of some fragments are difficult to describe accurately. We will further improve the automation of the whole

process. Although the number of fragments in the experiment is limited, the elements in the matrix can be expanded.

## REFERENCES


[1] N. Michael, B. Sabrina, and K. T. S. Sebastian, "New applications of 3D modeling in artefact analysis: Three case studies of viking age brooches," *Archaeolog. Anthropolog. Sci.*, vol. 8, p. 4, pp. 651–662, 2016, doi: 10.1007/s12520-014-0200-9.

[2] L. Arbace, E. Sonnino, M. Callieri, M. Dellepiane, M. Fabbri, A. Iaccarino Idelson, and R. Scopigno, "Innovative uses of 3D digital technologies to assist the restoration of a fragmented terracotta statue," *J. Cultural Heritage*, vol. 14, no. 4, pp. 332–345, Jul. 2013, doi: 10.1016/j.culher.2012.06.008.

[3] M. Zhang, S. Chen, Z. Shu, S.-Q. Xin, J. Zhao, G. Jin, R. Zhang, and J. Beyerer, "Fast algorithm for 2D fragment assembly based on partial EMD," *Vis. Comput.*, vol. 33, no. 12, pp. 1601–1612, Dec. 2017, doi: 10.1007/s00371-016-1303-3.

[4] A. Kanezaki, T. Harada, and Y. Kuniyoshi, "Partial matching of real textured 3D objects using color cubic higher-order local auto-correlation features," *Vis. Comput.*, vol. 26, no. 10, pp. 1269–1281, Oct. 2010, doi: 10.1007/s00371-010-0521-3.

[5] R. Pintus, K. Pal, Y. Yang, T. Weyrich, E. Gobbetti, and H. Rushmeier, "A survey of geometric analysis in cultural heritage: Geometric analysis in cultural heritage," *Comput. Graph. Forum*, vol. 35, no. 1, pp. 4–31, Feb. 2016, doi: 10.1111/cgf.12668.

[6] F. Cohen, Z. Zhang, and Z. Liu, "Mending broken vessels a fusion between color markings and anchor points on surface breaks," *Multimedia Tools Appl.*, vol. 75, no. 7, pp. 3709–3732, Apr. 2016, doi: 10.1007/s11042-014-2190-0.

[7] K. Son, E. B. Almeida, and D. B. Cooper, "Axially symmetric 3D pots configuration system using axis of symmetry and break curve," in *Proc. IEEE Conf. Comput. Vis. Pattern Recognit.*, Jun. 2013, pp. 257–264. [Online]. Available: www.lems.brown.edu

[8] Y. Zheng, G. Li, S. Wu, Y. Liu, and Y. Gao, "Guided point cloud denoising via sharp feature skeletons," *Vis. Comput.*, vol. 33, nos. 6–8, pp. 857–867, Jun. 2017, doi: 10.1007/s00371-017-1391-8.

[9] R. R. Yager, "Bi-directional dominance for measure modeled uncertainty," *Inf. Sci.*, vol. 447, pp. 72–82, Jun. 2018, doi: 10.1016/j.ins.2018.01.050.

[10] W. Guo, C. Si, Y. Xue, Y. Mao, L. Wang, and Q. Wu, "A grouping particle swarm optimizer with Personal-Best-Position guidance for large scale optimization," *IEEE/ACM Trans. Comput. Biol. Bioinf.*, vol. 15, no. 6, pp. 1904–1915, Nov. 2018, doi: 10.1109/TCBB.2017.2701367.

[11] R. Fukushima, H. Wang, K. Tamura, J. Tsuchiya, and K. Yasuda, "Dominance relation-based genetic algorithm for superior solution set search problem," *IEEJ Trans. Electr. Electron. Eng.*, vol. 14, no. 6, pp. 959–960, Jun. 2019, doi: 10.1002/tee.22888.

[12] S. Bouamama, C. Blum, and A. Boukerram, "A population-based iterated greedy algorithm for the minimum weight vertex cover problem," *Appl. Soft Comput.*, vol. 12, no. 6, pp. 1632–1639, Jun. 2012, doi: 10.1016/j.asoc.2012.02.013.

[13] C. Walshaw, "Multilevel refinement for combinatorial optimisation problems," *Ann. Oper. Res.*, vol. 131, nos. 1–4, pp. 325–372, Oct. 2004, doi: 10.1023/B:ANOR.0000039525.80601.15.

[14] A. R. Malisia, "Improving the exploration ability of ant-based algorithms," in *Oppositional Concepts in Computational Intelligence* (Studies in Computational Intelligence), vol. 155, H. R. Tizhoosh and M. Ventresca, eds. Berlin, Germany: Springer, 2008, pp. 121–142, doi: 10.1007/978-3-540-70829-2_7.

[15] A. Borisenko and S. Gorlatch, "Comparing GPU-parallelized metaheuristics to branch-and-bound for batch plants optimization," *J. Supercomput.*, vol. 75, no. 12, pp. 7921–7933, Dec. 2019, doi: 10.1007/s11227-018-2472-9.

[16] W. Zhao, C. Du, and S. Jiang, "An adaptive multiscale approach for identifying multiple flaws based on XFEM and a discrete artificial fish swarm algorithm," *Comput. Methods Appl. Mech. Eng.*, vol. 339, pp. 341–357, Sep. 2018, doi: 10.1016/j.cma.2018.04.037.

[17] D. Yumin and Z. Li, "Quantum behaved particle swarm optimization algorithm based on artificial fish swarm," *Math. Problems Eng.*, vol. 2014, pp. 1–10, Jan. 2014, doi: 10.1155/2014/592682.

[18] C. B. Kalayci and C. Kaya, "An ant colony system empowered variable neighborhood search algorithm for the vehicle routing problem with simultaneous pickup and delivery," *Expert Syst. Appl.*, vol. 66, pp. 163–175, Dec. 2016, doi: 10.1016/j.eswa.2016.09.017.

[19] D. Arabadjis, C. Papaodysseus, P. Rousopoulos, and M. Panagopoulos, "On the mathematical formulation of the problem of reassembling fragmented objects: Two new theorems," *J. Appl. Math. Comput.*, vol. 34, nos. 1–2, pp. 81–100, Dec. 2010, doi: 10.1007/s12190-009-0308-8.

[20] Y. Xian, J. Xiao, and Y. Wang, "A fast registration algorithm of rock point cloud based on spherical projection and feature extraction," *Frontiers Comput. Sci.*, vol. 13, no. 1, pp. 170–182, Feb. 2019, doi: 10.1007/s11704-016-6191-1.

[21] Y. Wang, D. Ewert, D. Schilberg, and J. S. , "Edge extraction by merging the 3D point cloud and 2D image data," in *Automation, Communication and Cybernetics in Science and Engineering 2013/2014*. Springer, 2014, pp. 773–785, doi: 10.1007/978-3-319-08816-7_61.

[22] W. Zuo, D. Zhang, and K. Wang, "On kernel difference-weighted k-nearest neighbor classification," *Pattern Anal. Appl.*, vol. 11, nos. 3–4, pp. 247–257, Sep. 2008, doi: 10.1007/s10044-007-0100-z.

[23] T. R. Jones, F. Durand, and M. Desbrun, "Non-iterative, feature-preserving mesh smoothing," *ACM Trans. Graph.*, vol. 22, no. 3, p. 943, Jul. 2003. [Online]. Available: www.geometry.caltech.edu

[24] T.-W. Bae and K.-I. Sohng, "Small target detection using bilateral filter based on edge component," *J. Infr., Millim., THz Waves*, pp. 735–743, Mar. 2010, doi: 10.1007/s10762-010-9633-0.

[25] E. Altantsetseg, O. Khorloo, and K. Konno, "Rigid registration of noisy point clouds based on higher-dimensional error metrics," *Vis. Comput.*, vol. 34, nos. 6–8, pp. 1021–1030, Jun. 2018, doi: 10.1007/s00371-018-1534-6.

[26] M. Neshat, G. Sepidnam, M. Sargolzaei, and A. N. Toosi, "Artificial fish swarm algorithm: A survey of the state-of-the-art, hybridization, combinatorial and indicative applications," *Artif. Intell. Rev.*, vol. 42, no. 4, pp. 965–997, Dec. 2014, doi: 10.1007/s10462-012-9342-2.

[27] P. J. Besl and N. D. McKay, "A method for registration of 3-D shapes," *IEEE Trans. Pattern Anal. Mach. Intell.*, vol. 14, no. 2, pp. 239–256, Feb. 1992, doi: 10.1109/34.121791.

[28] X. Ge, "Non-rigid registration of 3D point clouds under isometric deformation," *ISPRS J. Photogramm. Remote Sens.*, vol. 121, pp. 192–202, Nov. 2016, doi: 10.1016/j.isprsjprs.2016.09.009.

[29] Q.-X. Huang, B. Adams, M. Wicke, and L. J. Guibas, "Non-rigid registration under isometric deformations," *Comput. Graph. Forum*, vol. 27, no. 5, pp. 1449–1457, Jul. 2008, doi: 10.1111/j.1467-8659.2008.01285.x.

[30] N. Mellado, D. Aiger, and N. J. Mitra, *Super 4PCS Fast Global Pointcloud Registration Via Smart Indexing*, vol. 33. Hoboken, NJ, USA: Wiley, 2014, pp. 205–215, doi: 10.1111/cgf.12446.

[31] M. Mohamad, M. T. Ahmed, D. Rappaport, and M. Greenspan, "Super generalized 4PCS for 3D registration," in *Proc. Int. Conf. 3D Vis.*, Oct. 2015, pp. 598–606, doi: 10.1109/3DV.2015.74.

[32] X. Wang and H. Zhu, "On the comparisons of unit dual quaternion and homogeneous transformation matrix," *Adv. Appl. Clifford Algebras*, vol. 24, no. 1, pp. 213–229, Mar. 2014, doi: 10.1007/s00006-013-0436-y.


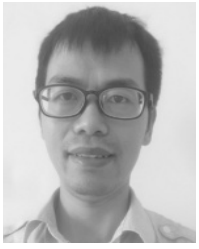

**ENSHENG LIU** was born in Ji'an, Jiangxi, China, in 1984. He received the B.S. and M.S. degrees in surveying and mapping engineering from the Jiangxi University of Science and Technology, Ganzhou, China. He is currently pursuing the Ph.D. degree in surveying and mapping science and technology with Tongji University, Shanghai, China. His research interests include least squares theory, 3D laser scanning point cloud data processing, theoretical method improvement of instrument calibration, and 3D model construction and application.

**XIAOJUN CHENG** was born in Jingdezhen, Jiangxi, China, in 1964. He received the B.S. degree in engineering surveying from Tongji University, Shanghai, China, in 1985, the M.S. degree, in 1992, and the Ph.D. degree in geodesy from Tongji University, in 2002.

Since 1985, he has been teaching with the College of Surveying and Geo-informatics, Tongji University, where he has also been a Professor, since 2002, and was appointed as a Ph.D. Supervisor the following year. He has published more than 200 articles and edited/co-edited 16 textbooks. His research interests include three-dimensional laser scanning technology, three-dimensional digital simulation, and precision engineering measurement.

Prof. Cheng chaired more than 40 projects of the National Natural Science Foundation of China, supervised more than 70 master's and Ph.D. students, won one first-class, three second-class and two third-class provincial and ministerial teaching achievement awards, and two second-class provincial and ministerial science and technology progress awards.

**XIAOLONG CHENG** received the B.S. degree in surveying and mapping engineering from the Henan University of Urban Construction, Henan, China, in 2009, the M.S. degree in geodesy and survey engineering from Nanjing Tech University, Nanjing, China, in 2012, and the Ph.D. degree in photogrammetry and remote sensing from Tongji University, Shanghai, China, in 2017. He is currently a Lecturer with the College of Architecture and Surveying and Mapping Engineering, Jiangxi University of Science and Technology, Ganzhou, China. His research interests include LiDAR data processing, multisource data fusion, and 3-D modeling.

**TENGFEI ZHOU** was born in Suizhou, Anhui, China, in 1993. He received the B.S. and M.S. degrees in surveying and mapping engineering from the Anhui University of Technology, Huainan, Anhui, in 2014 and 2017, respectively. He is currently pursuing the Ph.D. degree in surveying and mapping science and technology with Tongji University, Shanghai, China.

His research interests include least squares theory, 3D laser scanning point cloud data processing, theoretical method improvement of instrument calibration, and 3D model construction and application.

Mr. Zhou received the Second Prize of the 20th International Mining Measurement Forum, in 2017.

**YUHUA HUANG** was born in Ganzhou, Jiangxi, China, in 1985. She received the M.S. degree in Gannan Normal University, Ganzhou. Her research interests include archival research and computer image.